

# The coupling mechanism between crossed-beams energy transfer and stimulated Brillouin scattering in homogeneous plasmas

Y. Chen,<sup>1</sup> Q. Wang,<sup>2</sup> C. Y. Zheng,<sup>2,3,4</sup> Z. J. Liu,<sup>2,3</sup> L. H. Cao,<sup>2,3,4</sup> and C. Z. Xiao<sup>4,5, a)</sup>

<sup>1)</sup>*School of Electrical and Information Engineering, Anhui University of Science and Technology, Huainan, Anhui 232001, China*

<sup>2)</sup>*Institute of Applied Physics and Computational Mathematics, Beijing, 100094, China*

<sup>3)</sup>*HEDPS, Center for Applied Physics and Technology, Peking University, Beijing 100871, China*

<sup>4)</sup>*Collaborative Innovation Center of IFSA (CICIFSA), Shanghai Jiao Tong University, Shanghai 200240, China*

<sup>5)</sup>*Key Laboratory for Micro-/Nano-Optoelectronic Devices of Ministry of Education, School of Physics and Electronics, Hunan University, Changsha, 410082, China*

(Dated: 18 June 2024)

The coupling mechanism between crossed-beams energy transfer and stimulated Brillouin scattering in homogeneous plasmas are studied by theoretical analysis, fluid simulations and particle-in-cell(PIC) simulations. The numerical models of laser plasma instabilities are constructed by solving coupling equations with Schrödinger equation's form, and the fluid simulation results are confirmed by fluid theory and PIC simulations. In the parameter regime when the pump depletion does not occur in CBET and the reflectivity of SBS is lower than 1%, SBS will be affected by CBET, the CBET energy gain will still agree with theoretical predications. However, In the parameter regime when the pump depletion does occur in CBET and the reflectivity of SBS is higher than 1%, the CBET spatial gain will be reduced by the interaction of CBET and SBS, and the huge difference of SBS reflectivity for two crossed laser beams is observed. In the PIC simulations, we found that lower  $ZT_e/T_i$  will significantly reduce the interaction between CBET and SBS ( $Z$  is the ion charge,  $T_e$  is the electron temperature,  $T_i$  is the ion temperature).

## I. INTRODUCTION

Controlling the laser plasma instabilities is an important task in inertial confinement fusion (ICF)<sup>1-5</sup>, because the growth of these instabilities may affect the implosion symmetry of pellet compressing<sup>6,7</sup>. The crossed laser beams would induce the crossed-beams energy transfer when the phase match condition is satisfied. This instability is almost inevitable in ICF, however, people found that it is possible to tuning the implosion symmetry by CBET<sup>8-10</sup>.

The fluid theory and kinetic theory of CBET has been established, which are also confirmed by experiments<sup>11-16</sup>. However, recent researches reported that the CBET will induce stimulated forward Raman scattering (SFRS) at high laser intensity regime, which make the CBET gain have gap with theoretical predictions<sup>17,18</sup>. Also, the hot electrons produced by SFRS may be harmful to fusion<sup>19</sup>. We should note that SFRS is induced when the laser beams are multi-speckled structures, in this paper, we use the ordinary Gaussian type laser beams, the SFRS is not observed. Inspired by these works, we predict that the CBET would also influence the reflectivity of stimulated Brillouin scattering (SBS), at the limit when pump depletion of CBET occurs, the increased SBS reflectivity may affect the CBET spatial gain. This issue is important because the SBS can seriously consume the laser energy<sup>20-31</sup>.

The fluid simulations<sup>32,33</sup> and particle in cell (PIC)<sup>34</sup> are two important methods to simulate CBET process, the fluid simulations focus on the wave-wave interactions, and the advantage is that it can save computational time. The advantage of PIC simulation is that it can consider the kinetic effects on instabilities. At low temperature of plasma regime, the kinetic

effects is weak, so, the fluid simulations are more suitable for the instabilities in fluid regime.

In this paper, in order to implement long-time CBET and SBS simulations, we developed a wave based program for CBET and SBS in fluid regime. It solve the coupling equations of CBET and SBS by Du Fort-Frankel Scheme, This code can save much more computation time than PIC simulations, and it can ensure accuracy even in sparse spatial mesh. Then, we use fluid simulations to study the coupling mechanism between CBET and SBS, by turning on or turning off one instability, one can clearly observe the influence of one instability on another.

In our theoretical analysis, the parameters space of CBET gain is divided to two regimes, the trivial regime and depletion regime (define later), the parameters space of SBS gain is also divided to two regimes, (1) the regime when the SBS reflectivity is lower than 1%, (2) the regime when the SBS reflectivity is higher than 1%. At the trivial regime of CBET and  $R_{sbs} < 1\%$  regime, SBS reflectivity will be affected by CBET, but the CBET energy gain won't be seriously affected by SBS. However, in the depletion regime of CBET and the  $R_{sbs} > 1\%$  regime, the pump depletion of CBET can significantly increase SBS reflectivity, the huge difference of the SBS reflectivity for crossed beams is observed. Also, the CBET gain will be inconsistent with fluid theory in depletion regime because of the interaction between CBET and SBS. At last, the PIC simulations agree with our fluid simulations. As the decreases of  $ZT_e/T_i$ , the IAWs in SBS will be strongly damped, then the interaction between CBET and SBS will become weaker. As the increase of intensities of laser beams, the coupling mechanism between CBET and other instabilities should get attention, because it may make the experimental result deviate from CBET theoretical predictions.

This paper is structured in the following ways. Firstly, in

<sup>a)</sup>Electronic mail: xiaocz@hnu.edu.cn

Sec. II, we describe the fluid model of CBET and SBS with coupling equations in Schrödinger equation's form. Then, we propose the numerical solutions for the coupling equation. Secondly, The theoretical analysis and simulations are performed in Sec. III. At last, the conclusion and discussion about the sinusoidal density modulation are shown in Sec. IV.

## II. NUMERICAL ALGORITHM OF SBS COUPLING EQUATIONS

As we know, CBET can be considered as a special case of SBS process, occurring when multi laser beams overlap in plasma, thus, CBET and SBS share the coupling equations,

$$(\partial_t^2 - c^2 \nabla^2 + \omega_{pe}^2) A_0 = -\frac{4\pi e^2}{m_e} \tilde{n}_e A_1, \quad (1)$$

$$(\partial_t^2 - c^2 \nabla^2 + \omega_{pe}^2) A_1 = -\frac{4\pi e^2}{m_e} \tilde{n}_e A_0, \quad (2)$$

$$[(\partial_t + V \cdot \nabla)^2 - C_s^2 \nabla^2] \tilde{n}_e = \frac{Z n_0 e^2}{m_e m_i c^2} \nabla^2 (A_0 \cdot A_1), \quad (3)$$

where  $A_0$  is the vector potential of pump laser for CBET(SBS),  $A_1$  is the vector potential of seed laser for CBET(SBS),  $c$  is the velocity of light in vacuum,  $\tilde{n}_e$  is the plasma density perturbation of ion acoustic wave.  $n_0$  and  $\omega_{pe}$  are the density and electron density and plasma frequency,  $m_e$  and  $m_i$  are the mass of electron and ion, respectively  $Z$  is the charge state of ion, and  $C_s$  is the ion-sound velocity.

The intensities of laser beams in ICF are in the range of  $10^{14} \sim 10^{15}$  W/cm<sup>2</sup>, so, the characteristic time of SBS can be obtained by  $\tau = 1/\gamma_0$ , which is around hundreds of times of pump laser's period, where  $\gamma_0$  is the growth rate of SBS in homogenous plasma. Thus, the three waves of SBS can be expressed as the product of a slowly-changing envelope in time and a rapidly oscillating periodic function,

$$\begin{aligned} A_0(x, t) &= \frac{1}{2} \tilde{A}_0(x, t) e^{-i\omega_0 t + i\vec{k}_0 \cdot r} + c.c. \\ A_1(x, t) &= \frac{1}{2} \tilde{A}_1(x, t) e^{-i\omega_1 t + i\vec{k}_1 \cdot r} + c.c. \\ \tilde{n}_e(x, t) &= \frac{1}{2} \delta \tilde{n}_e(x, t) e^{-i\omega_2 t + i\vec{k}_2 \cdot r} + c.c. \end{aligned} \quad (4)$$

where  $\omega_0$  is the frequency of pump laser,  $\omega_1$  is the frequency of seed laser and  $\omega_2$  is the frequency of IAW. Substituting Eq. (4) to Eq. (1-3), Then, we obtain the coupling equations with Schrödinger equation's form,

$$\partial_t a_0 = \frac{i}{2} [\nabla^2 + (1 - n_0)] a_0 - \frac{i}{4} \tilde{n}_e a_1, \quad (5)$$

$$\partial_t a_1 = \frac{i}{2} \frac{\omega_0}{\omega_1} \left[ \nabla^2 + \left( \frac{\omega_0^2}{\omega_1^2} - n_0 \right) \right] a_1 - \frac{i}{4} \frac{\omega_0}{\omega_1} \tilde{n}_e^* a_0, \quad (6)$$

$$\begin{aligned} \partial_t \tilde{n}_e &= \frac{i}{2} \frac{\omega_0}{\omega_{20}} \left[ \frac{C_s^2}{c^2} \nabla^2 + \frac{\omega_2^2}{\omega_0^2} - \frac{V_x^2}{c^2} \partial_x^2 - \frac{V_y^2}{c^2} \partial_y^2 \right] \tilde{n}_e \\ &\quad - \frac{\omega_2}{\omega_{20}} \left( \frac{V_x}{c} \partial_x + \frac{V_y}{c} \partial_y \right) \tilde{n}_e - (v + i\delta\omega) \tilde{n}_e \\ &\quad + \frac{i}{4} \frac{Z n_0 m_e \omega_0}{m_i \omega_{20}} \nabla^2 (a_1^* \cdot a_0), \end{aligned} \quad (7)$$

where  $a_0 = \frac{eA_0}{m_e c^2}$ ,  $a_1 = \frac{eA_1}{m_e c^2}$ ,  $\tilde{n}_e$  and  $n_0$  have been normalized to the critical density of pump laser  $n_c$ , the space is normalized to  $c/\omega_0$ , time is normalized to  $\omega_0^{-1}$ ,  $V_x$  and  $V_y$  are the components of flowing velocities of plasma at each axis. It should be noted that  $\omega_{20}$  is frequency of IAW when the flowing velocity of plasma reaches to zero. We also phenomenally add the Landau damping  $v$  and the nonlinear frequency shift of IAW  $\delta\omega$  in Eq. (7), where the Landau damping of IAW is

$$v = \frac{\omega_{20}}{\omega_0} \left[ \sqrt{\frac{Z m_e}{m_i}} + \left( \left( \frac{Z T_e}{T_i} \right)^{\frac{3}{2}} e^{-\frac{(C_s - V)^2}{2v_i^2}} \right) \right] / (1 + k^2 \lambda_{De}^2)^{\frac{3}{2}}, \quad (8)$$

where  $\lambda_{De}$  is the Debye length of plasma. The nonlinear frequency shift of IAW  $\delta\omega$  can be expressed as<sup>35</sup>

$$\delta\omega = -\frac{1}{\sqrt{2\pi}} \left[ \alpha_i \sqrt{\frac{Z T_e}{T_i}} (\zeta^4 - \zeta^2) e^{-\frac{\zeta^2}{2}} - \alpha_e \right] |\tilde{n}_e/n_0|^{\frac{1}{2}}, \quad (9)$$

the parameters  $\alpha_e = 0.544$ ,  $\alpha_i = 0.823$ , which stands for the contributions to the frequency shift from electrons and ions<sup>36</sup>, where  $\zeta = C_s/v_{thi}$ ,  $v_{thi} = \sqrt{T_i/m_i}$ .

If the flowing velocity of plasma and the ion sound velocity cancel each other out, *i.e.*  $C_s = \sqrt{V_x^2 + V_y^2}$ , then the Eq. (7) becomes

$$\partial_t \tilde{n}_e = -(v + i\delta\omega) \tilde{n}_e + \frac{i}{4} \frac{Z n_0 m_e \omega_0}{m_i \omega_{20}} \nabla^2 (a_1^* \cdot a_0), \quad (10)$$

thus the IAW becomes a stationary wave. In addition, if there is no flowing velocity of plasma, *i.e.*  $V = 0$ , the the Eq. (7) becomes

$$\begin{aligned} \partial_t \tilde{n}_e &= \frac{i}{2} \frac{\omega_0}{\omega_{20}} \left[ \frac{C_s^2}{c^2} \nabla^2 + \frac{\omega_{20}^2}{\omega_0^2} \right] \tilde{n}_e - (v + i\delta\omega) \tilde{n}_e \\ &\quad + \frac{i}{4} \frac{Z n_0 m_e \omega_0}{m_i \omega_{20}} \nabla^2 (a_1^* \cdot a_0), \end{aligned} \quad (11)$$

### A. Du Fort-Frankel Scheme for SBS coupling equations

We developed a parallel program called WEBS (Wave Based Simulations), this code focusing on solving coupling equations of laser plasma instabilities. In this paper, we use Du Fort-Frankel scheme to numerically solve Eq. (5-7). WEBS can also be used to simulate other instabilities, such as stimulated Raman scattering (SRS), two plasma decay (TPD)<sup>37</sup> and laser self-focusing.

Du Fort-Frankel scheme was proposed to numerically solve second order parabolic differential equations in 1953<sup>38</sup>, and it

has been adopted to solve other nonlinear problem<sup>39,40</sup>. The truncation error of this scheme is  $O(\Delta t^2/h^2)$ <sup>41</sup>, where  $\Delta t$  and  $h$  are the size of the grid mesh in time and space, early research has proved that the Du Fort-Frankel scheme is unconditionally stable and it has second order accuracy<sup>42</sup>. Similar to leap-frog schemes and symplectic algorithm<sup>43,44</sup>, our code WEBS can nearly conserve the total energy in long-time simulations, which is very suitable for CBET and SBS simulations.

The detail of Du Fort-Frankel scheme in WEBS can be seen in Appendix. A, In Eq. (A1-A3), one can observe that the updating of wave's value at  $(i, j)$  are only related to the wave's values around it, which makes our code suitable for parallel programming.

## B. Benchmark of WEBS simulation against PIC simulations

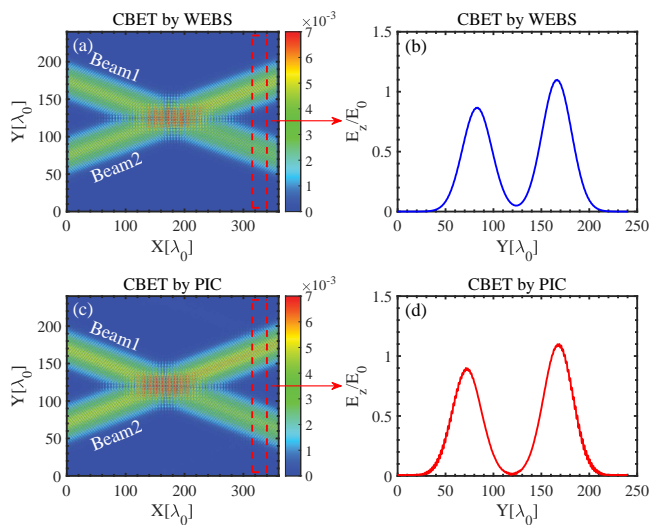


FIG. 1. The comparison between WEBS simulation results and PIC simulation results. (a) The amplitude of laser at  $t = 6.6\text{ps}$  by WEBS simulation. (b) the normalized amplitude of two lasers after CBET, the results are obtained by the integral of  $x$  in the red rectangle of (a). (c) The amplitude of laser at  $t = 6.6\text{ps}$  by PIC simulation. (d) the normalized amplitude of two lasers after CBET, the results are obtained by the integral of  $x$  in the red rectangle of (c).

In this subsection, we compare the CBET results of WEBS with that in PIC simulations, the PIC code we use here is EPOCH<sup>34</sup>. Considering a CBET process in two-dimensional (2D) system, two crossed Gaussian laser beams are injected into the system from the left hand side of simulation box, the crossed angle is  $31^\circ$ , the maximum intensities of these laser beam are both  $3 \times 10^{14}\text{W/cm}^2$ , the Half height full width at lateral direction of laser beam is  $20\lambda_0$ , where  $\lambda_0 = 0.351\mu\text{m}$  is the wavelength of pump laser of CBET. The simulation box is  $L_x = 360\lambda_0$ ,  $L_y = 240\lambda_0$ , the plasma density in this paper is  $0.05n_c$ , where  $n_c$  is the critical density of pump laser. The plasma we used in this paper is He, with  $Z = 2$  and  $m_i = 7344m_e$ . The temperatures of electron and ion are  $T_e = 1\text{keV}$ ,  $T_i = 0.2\text{keV}$ . For resonantly excites CBET, the

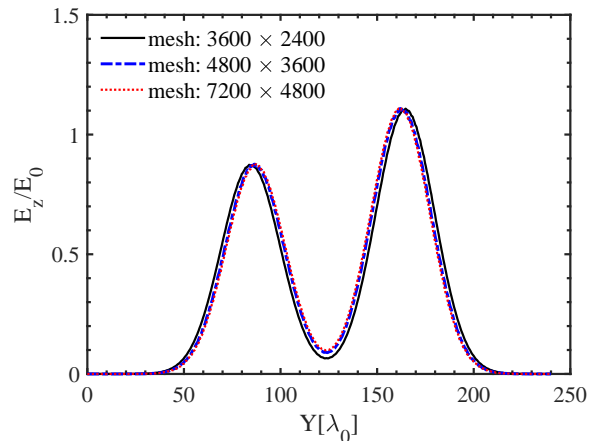


FIG. 2. The results of WEBS for different spatial mesh. The parameters of lasers and plasma are same to that in Fig 1. The black line is the amplitude of two laser at  $t = 6.6\text{ps}$  by  $3600 \times 2400$  mesh. The blue dashed line is the amplitude of two laser at  $t = 6.6\text{ps}$  by  $4800 \times 3600$  mesh. The red dot line is the amplitude of two laser at  $t = 6.6\text{ps}$  by  $7200 \times 4800$  mesh.

wavelength of seed laser is  $\lambda_1 = 0.35115234\mu\text{m}$ . In the PIC simulation, there is 10 cells in each  $\lambda_0$  and the number of particles in per cell (PPC) is 100, other parameters of laser and plasma are the same to that in WEBS simulations.

In Fig 1 (a) and (c), the normalized amplitude of lasers are shown, the results of WEBS and PIC share the same features, the intensity of pump laser reduces because the energy is transferred by CBET in the laser overlap region. We select the simulation area marked by red dashed lines in Fig 1 (a) and (c) to determine how much the laser's amplitudes changes after CBET, as shown in Fig 1 (b) and (d), the maximum amplitude of pump laser and seed laser in WEBS are consistent with that in PIC simulation. We note that the results of WEBS in Fig 1 are obtained by using spatial mesh,  $7200 \times 4800$ .

In addition, it is necessary to compare the results with different spatial mesh, as shown in Fig 2, the black lines is the amplitudes of laser by WEBS with mesh  $3600 \times 2400$ , the blue dashed lines is the amplitudes of laser by WEBS with mesh  $4800 \times 3600$ , the red dotted lines is the amplitudes of laser by WEBS with mesh  $7200 \times 4800$ , The results with different mesh are consistent with each other, so, one can save computation cost by reducing the spatial mesh in WEBS simulations, at the same time, the physical results are unchanged. In the rest of this paper, the spatial mesh,  $7200 \times 4800$  is used in WEBS. In the next section, we also compare our simulation results with CBET fluid theory.

## III. THE INTERACTION BETWEEN CBET AND SBS

As the growth of CBET in ICF, the difference of intensities will occur in crossed laser beams, which causes different gains of other instabilities (such as SRS, SBS, TPD) in the path of different beams. Recent researches have showed clear evidences of stimulated forward Raman scattering (SFRS) by

PIC simulations, and the energy of laser beams was depleted by SFRS, at the same time, the massive productions of hot electrons because of SFRS are detrimental for ignition[1]. We predicted that CBET can cause significant difference of reflectivity of SBS for crossed laser beams. In this sections, we will study the interactions between CBET and SBS in homogenous plasma by theoretical analysis and simulations.

### A. theoretical coupling model of CBET and SBS

For simplicity, we consider two crossed laser beams with the crossed angle  $\theta$  and the frequency of these two beams satisfy the phase match condition of CBET,  $\omega_0 = \omega_1 + \omega_2$ , where  $\omega_0$  and  $\omega_1$  are the frequency of Beam1 and Beam2, respectively.  $\omega_2 = k_2 C_s - \vec{k}_2 \cdot \vec{V}$  is the frequency of IAW in CBET, CBET will growth at the intersection point of laser beams. Besides, we should also consider the SBS process for each laser beam, we denote the frequency of Beam1's SBS reflected light is  $\omega_3$ , and the frequency of IAW is  $\omega_5$ . The frequency of Beam1's SBS reflected light and IAW are  $\omega_4$  and  $\omega_6$ , respectively. Thus, we can write the coupling equations of CBET and SBS,

$$(\partial_t^2 - c^2 \nabla^2 + \omega_{pe}^2) A_0 = -\frac{4\pi e^2}{m_e} (\tilde{n}_{e2} A_1 + \tilde{n}_{e5} A_3), \quad (12)$$

$$(\partial_t^2 - c^2 \nabla^2 + \omega_{pe}^2) A_1 = -\frac{4\pi e^2}{m_e} (\tilde{n}_{e2} A_0 + \tilde{n}_{e6} A_4), \quad (13)$$

$$[(\partial_t + V \cdot \nabla)^2 - C_s^2 \nabla^2] \tilde{n}_{e2} = \frac{Z n_0 e^2}{m_e m_i c^2} \nabla^2 (A_0 \cdot A_1), \quad (14)$$

$$(\partial_t^2 - c^2 \nabla^2 + \omega_{pe}^2) A_3 = -\frac{4\pi e^2}{m_e} \tilde{n}_{e5} A_0, \quad (15)$$

$$(\partial_t^2 - c^2 \nabla^2 + \omega_{pe}^2) A_4 = -\frac{4\pi e^2}{m_e} \tilde{n}_{e6} A_1, \quad (16)$$

$$[(\partial_t + V \cdot \nabla)^2 - C_s^2 \nabla^2] \tilde{n}_{e5} = \frac{Z n_0 e^2}{m_e m_i c^2} \nabla^2 (A_0 \cdot A_3), \quad (17)$$

$$[(\partial_t + V \cdot \nabla)^2 - C_s^2 \nabla^2] \tilde{n}_{e6} = \frac{Z n_0 e^2}{m_e m_i c^2} \nabla^2 (A_1 \cdot A_4), \quad (18)$$

where  $A_0, A_1, \tilde{n}_{e2}$  belong to the CBET process,  $A_0, A_3, \tilde{n}_{e5}$  belong to the SBS process of Beam1,  $A_1, A_4, \tilde{n}_{e6}$  belong to the SBS process of Beam2.

Based on the coupling equations of CBET and SBS, we predict that the pump depletion by CBET plays an important role in the interaction between CBET and SBS. When the pump depletion by CBET occur, the reflectivity of SBS for each beams will have huge difference because of the unequal intensities for Beam1 and Beam2. However, when the

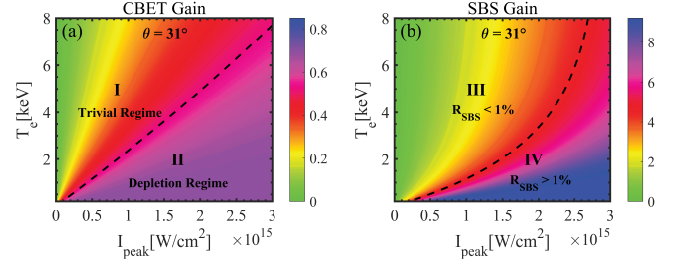


FIG. 3. The theoretical CBET gain for different parameters. The results are obtained by Eq. (24). I stands for trivial regime of CBET, II stands for the depletion regime. (a) The CBET gain for different electron temperature and laser intensities when  $\theta = 31^\circ$ . (b) The SBS gain for different electron temperature and laser intensities. III stands for the regime when the reflectivity is lower than 1%, IV stands for the regime when the reflectivity is higher than 1%.

CBET process does not significantly change the intensities of laser beams, *i.e.* pump depletion by CBET does not occur, the CBET and SBS will grow independently. Now, the crucial point is to determine the parameter space for the pump depletion of CBET. The fluid theory of CBET is frequently used to study the CBET processes in ICF<sup>11</sup>, so, we reuse the fluid theory of CBET to obtain the gain of CBET. In our model, the intensity growth of Beam2 along its path  $\ell$  is,

$$I_1 = I_{10} \exp \left[ \int L_{\text{CBET}}^{-1} d\ell \right], \quad (19)$$

where  $I_{10}$  is the original intensity of Beam2,  $L_{\text{CBET}}$  is the scale-length of energy gain by CBET,  $L_{\text{CBET}}^{-1}$  can be obtained by

$$L_{\text{CBET}}^{-1} = \frac{k_0}{4} \frac{n_0}{n_c - n_0} \left( \frac{\bar{v}_{\text{osc}}}{v_e} \right)^2 \left[ (1 + 3T_i/ZT_e) \frac{v_2}{\omega_{20}} \right] P(\eta), \quad (20)$$

where  $v_2$  is the Landau damping of IAW,  $\bar{v}_{\text{osc}}$  is the average normalized amplitude over the width of Gaussian lasers,  $d = 90\lambda_0$ , and  $P(\eta)$  is defined by

$$P(\eta) = \frac{(v_2/\omega_{20})^2 \eta}{(\eta^2 - 1)^2 + (v_2/\omega_{20})^2 \eta^2}, \quad (21)$$

the  $\eta$  is the modifying coefficient of IAW frequency because of the flowing velocity of plasma,  $\eta = \vec{k}_2 \cdot \vec{V} / \omega_{20} + \omega_2 / \omega_{20}$ . From Eq. (19), the energy gain of CBET can be expressed as

$$G_0 = \int L_{\text{CBET}}^{-1} d\ell, \quad (22)$$

which is the spatial gain of Beam2 along the path  $\ell$ . In the homogenous plasma,  $L_{\text{CBET}}^{-1}$  is a constant, then the Eq. (22) can be reduced to

$$G_0 = L_{\text{CBET}}^{-1} \cdot L_c, \quad (23)$$

where  $L_c = d/\sin\theta$  is the reduction of interaction length of CBET.

However, this equation dose not consider the influence of pump depletion, we should use Tang formula<sup>45</sup> to obtain the final energy gain

$$G_{Tang} = \ln \left[ \frac{(1 + \beta)e^{G_0(1+\beta)}}{1 + \beta e^{G_0(1+\beta)}} \right], \quad (24)$$

where  $\beta = I_{10}/I_0$ , is the seed level for CBET, in our model, we assume that two crossed laser beams have the same intensity, so,  $\beta = 1$ .

We note that this scheme is also suitable for calculating the spatial gain of SBS, one needs to change Eq. (19-24) to make them suitable for SBS.

As an example, let's consider two Gaussian laser with the same intensities, the width of laser is  $90\lambda_0$  the crossed angle is set as  $31^\circ$ . The density of plasma is  $0.05n_c$ , the temperature of electron  $T_e$  is varied, as shown in Fig 3, and the temperature of ions is  $T_i = T_e/5$ . The path length of SBS reflected light is  $L/\cos(\theta/2)$ , where  $L = 360\lambda_0$  is the length of plasma region. The seed level of SBS reflected light is  $10^{-4}$ .

In Fig 3, we obtain the CBET spatial gain and SBS spatial gain for different intensities and electron temperatures, Fig 3 (a) is for the CBET only case, and Fig 3 (b) is for the SBS only case. one can observe that the SBS spatial gain are much larger than CBET spatial gain, because the seed level of CBET is 1, which is much larger than that in SBS. There will be 70% energy of Beam1 is transferred to Beam2 only when the CBET gain is 0.531, so, we assume that the pump depletion occurs when  $G_{Tang} \approx 0.531$ . As shown in Fig 3 (a), the parameter space is divided into two regimes, (I): the trivial regime, and (II): the depletion regime. We can predicate that CBET has minor impact on SBS in the trivial regime, and CBET has significant impact on SBS. Similarly, we also divide the parameter space of SBS into two regimes, (III): the reflectivity of SBS is lower than 1%, (IV): the reflectivity of SBS is larger than 1%. The SBS is not able to affect the CBET gain in regime (III). However, at regime (IV), SBS will reduce the CBET gain because  $R_{SBS} > 1\%$ .

If the laser intensities and  $T_e$  locate at regime (I) and (III), the influence of SBS on CBET gain is negligible, we predicate the CBET gain will Conform to fluid theory, and the SBS reflectivity can still be obtained by fluid theory, one need to consider the SBS processes in front of CBET region and behind CBET region, respectively, because the laser intensities of laser beams are different in SBS.

If the laser intensities and  $T_e$  locate at regime (II) and (III), we should consider the SBS processes at two region: (i) the region in front of lasers beams crossed region, the length is  $\frac{1}{2}L_{sbs}$ , (ii) the region behind the lasers beams crossed region, the length is also  $\frac{1}{2}L_{sbs}$ . Assuming the intensity of Beam1 becomes 0, the intensity of Beam2 becomes  $2I_{10}$ . Thus, the SBS gain<sup>46,47</sup> for Beam1 and Beam2 are

$$G_{b1} = \frac{1}{2}G_b, G_{b2} = \frac{3}{2}G_b, \quad (25)$$

where  $G_b$  is the spatial gain of SBS in SBS only case. Thus, if the pump depletion occur in CBET, the ratio of convective

SBS reflectivity for two laser beams is

$$\frac{R_1}{R_2} = \frac{e^{\frac{1}{2}G_b}}{e^{\frac{3}{2}G_b}} = 1 : e^{G_b}. \quad (26)$$

However, if the laser intensities and  $T_e$  locate at regime (II) and (IV), the situation becomes more complicated, the growth of SBS will affect CBET gain, and the CBET will also affect the SBS reflectivity. At this regime, the CBET gain will not agree with fluid theory, and the difference in SBS reflectivity between two laser beams will be significant.

The analysis above is about convective SBS, it does not consider the situation when SBS is in the absolute regime<sup>48</sup>, when

$$\gamma_0 > \frac{\sqrt{|v_{g4}v_{g6}|}}{2} \left( \frac{v_6}{v_{g6}} \right), \gamma_0 > \frac{\sqrt{|v_{g3}v_{g5}|}}{2} \left( \frac{v_5}{v_{g5}} \right), \quad (27)$$

the growth of IAW in absolute regime is exponential as time, one can not use Eq. (25) to calculate the SBS reflectivity of laser beams.

In the next subsection, we will use numerical simulations to discuss the interaction between CBET and SBS.

## B. Fluid simulations for CBET and SBS interaction

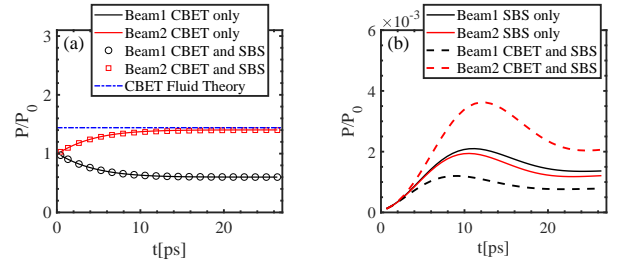


FIG. 4. The results of WEBS simulations. The intensities of laser is  $1 \times 10^{15} \text{W/cm}^2$ , the electron temperature is 4keV. (a) The time-dependent lasers' energy for different cases. The red line and black line belong to the CBET only case, the blue dashed line obtained by CBET fluid theory, the red squares and black circles belong to the CBET and SBS case. (b) The time-dependent SBS reflectivity for lasers in different cases. The red line and black line belong to the SBS only case, and the red dashed line and black dashed line belong to the CBET and SBS case.

At this subsection, we use fluid simulations to study the interaction between CBET and SBS. the intensities of two laser beams can be changed from  $1 \times 10^{14} \text{W/cm}^2$  to  $1.3 \times 10^{15} \text{W/cm}^2$ , the electron temperatures can be changed from 0.5keV to 5keV, and we set the seed level of SBS as  $10^{-4}I_0$  to reduce the simulation time. The total simulation time is 26.4ps to make sure the system has reached steady state.

First, we consider a simple case when the parameters for CBET locate at the regime (I) in Fig 3 (a), and the parameters for SBS locate at the regime (III) in Fig 3 (b). The intensities of two lasers are both  $1 \times 10^{15} \text{W/cm}^2$ , the electron temperature is 4keV, the temperature of ions is still  $T_e/5$ . We carry out

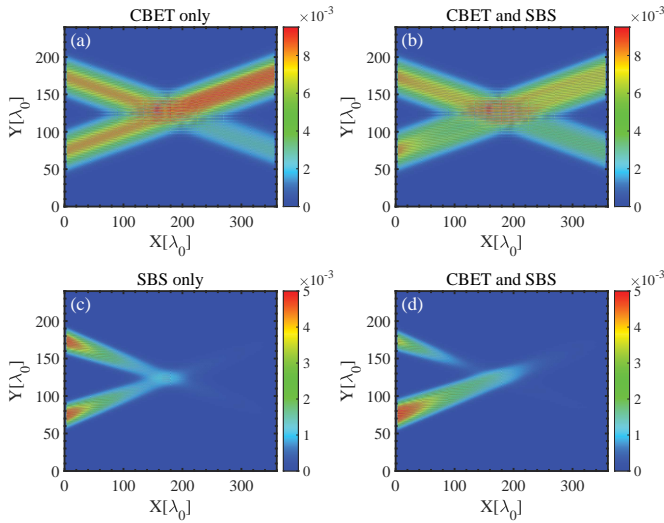


FIG. 5. The results by WEBS simulations. (a) The amplitude of lasers at  $t = 13.2\text{ps}$  in CBET only case. (b) The amplitude of lasers at  $t = 13.2\text{ps}$  in CBET and SBS case. (c) The amplitude of SBS reflected light at  $t = 13.2\text{ps}$  in SBS only case. (d) The amplitude of SBS reflected light at  $t = 13.2\text{ps}$  in CBET and SBS case.

three WEBS simulations, CBET only case, SBS only case and CBET and SBS case. As shown in Fig 4 (a), the black line and red line are the time dependent laser energy for Beam1 and Beam2 in the CBET only case, the SBS processes are turned off, one can observe that the simulation results agree with the CBET fluid theory prediction (blue dashed line). In Fig 4 (b), the black line and red line are the time dependent SBS reflectivity for Beam1 and Beam2 in SBS only case, they basically remain the same. The slight difference stems from the difference in Landau damping of IAWs. Then, we turn on the CBET and SBS processes, the black circles and red squares are the time dependent laser energy for Beam1 and Beam2 in the CBET and SBS case, as discussed above, the parameters locate at the regime (I) and regime (III), the SBS reflectivity is too small to affect the CBET gain, thus the energy transferring can still be predicted by CBET fluid theory. The SBS reflectivity for Beam1 and Beam2 in CBET and SBS case are shown by black dashed line and red dashed line in Fig 4 (b), the SBS reflectivity of Beam2 is larger than that of Beam1.

Now, we consider the case whose parameters locate at different regimes, the laser intensities are still  $1 \times 10^{15}\text{W}/\text{cm}^2$ , the electron temperature is  $1\text{keV}$ , the ion temperature is also  $T_e/5$ . Based on theoretical predictions, the CBET gain locate at regime (II), and the SBS gain locate at regime (IV). The CBET process and SBS processes will interact with each other, when the system reaches steady state, the CBET spatial gain won't agree with CBET fluid theory.

A significant advantage about WEBS is that one can easily turn off one physical process to study the individual evolution process of another physical process, then one turn on the physical process to study the interaction. For example, in Fig 5 (a), we turn off the SBS process, there is only CBET process left, one can clearly see that the energy of Beam1 is

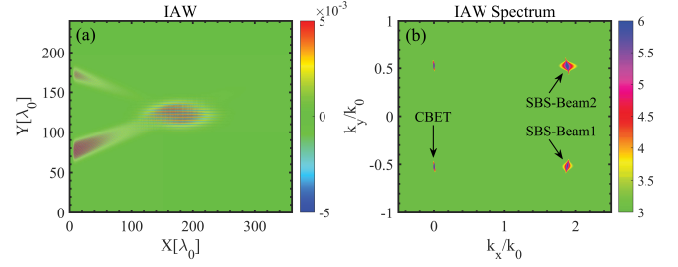


FIG. 6. The results of CBET and SBS case by WEBS simulations. (a) the amplitude of IAW in CBET and SBS case at  $t = 13.2\text{ps}$ . (b) The corresponding spectrum in  $k$  space.

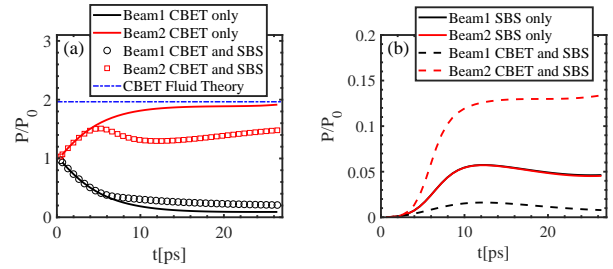


FIG. 7. The results of WEBS simulations. (a) The time-dependent lasers' energy for different cases. The red line and black line belong to the CBET only case, the blue dashed line obtained by CBET fluid theory, the red dashed line and black dashed line belong to the CBET and SBS case. (b) The time-dependent SBS reflectivity for lasers in different cases. The red line and black line belong to the SBS only case, and the red dashed line and black dashed line belong to the CBET and SBS case.

transferred to Beam2 by CBET. Similarly, as shown in Fig 5 (c) we only retain the SBS process, the SBS reflected lights for Beam1 and Beam2 are symmetrical and the reflectivity is the same. However, in Fig 5 (b) and (d), the SBS and CBET are both turned on, one can clearly see that the SBS will reduce the energy gain of CBET about 50%, and the existence of CBET introduces asymmetric SBS reflected light for Beam1 and Beam2.

The similar features also exist in the IAW of CBET and SBS, as shown in Fig 6 (a), the IAW at the center of the simulation box belongs to CBET, and the IAWs at the left hand side come from Beam1 and Beam2's SBS processes, one can observe that the amplitude of Beam2's IAW is larger than that of Beam1's, the reason is that CBET changes the SBS's growth rate, the same features are clearly shown in the spectrum of IAW in  $k$  space shown in Fig 6 (b).

Fig 7 (a) is the time dependence of laser beams' energy, the red line and black line belong to the CBET only case, around 20ps, it comes into steady state, the energy of Beam2 is consistent with CBET fluid theory (blue dashed line), and the energy of Beam1 is close to 0, which is the clear characteristic of pump depletion. The red squares and black circles belong to the CBET and SBS case, we observe that the pump depletion of Beam1 still exists, but the energy gain of

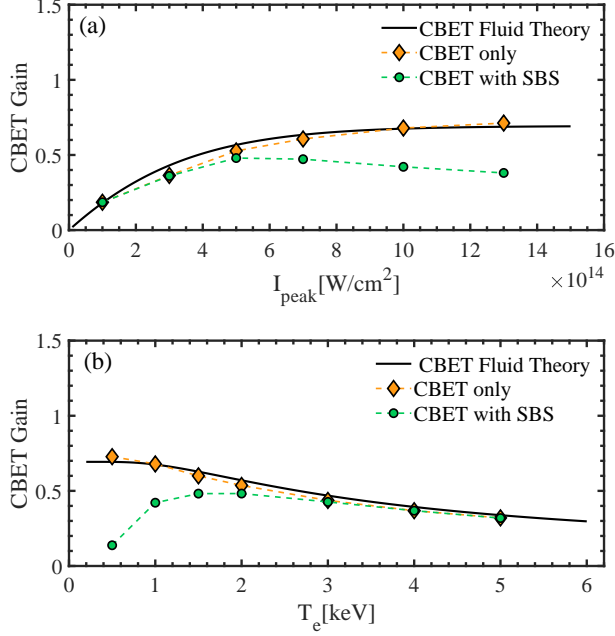


FIG. 8. The simulation results by WEBS. (a) The laser intensities-dependent CBET gain, the orange diamonds are the results of CBET only case. the green dots stands for the results of CBET and SBS case. The black line is obtained by CBET fluid theory. (b) The plasma temperature-dependent CBET gain, the orange diamonds are the results of CBET only case. the green dots stands for the results of CBET and SBS case. The black line is obtained by CBET fluid theory.

Beam2 reduces, because the the SBS consumes much energy of Beam2.

Fig 7 (b) is the time depended of SBS reflectivity for laser beams. the red line and black line belong to the SBS only case, the reflectivity of Beam1 and Beam2 are the same, which agrees with our predication. The red dashed line and black dashed line belong to the CBET and SBS case, we can clearly see the huge difference between Beam1 and Beam2, the reason is that the intensity of Beam1 is above absolute threshold, the IAW exponentially growth as time, which makes the reflectivity much larger than Beam1. In Fig 7 (b), If we ignore the interaction between CBET and SBS, the average total SBS reflectivity for Beam1 and Beam2 is 8.05%, in the CBET and SBS case, average total SBS reflectivity for Beam1 and Beam2 is 11.01%, the total SBS reflectivity increases because the interaction between CBET and SBS.

Next, we discuss the CBET spatial gain for different laser and plasma parameters, as shown in Fig 8 (a), the orange diamonds are the CBET gain of CBET only case, CBET gain increases with the intensity of lasers, when the peak intensity of laser reaches to  $1.3 \times 10^{15} \text{W/cm}^2$ , the intensity of Beam2 will be nearly doubled because of pump depletion. And the simulation results of WEBS for CBET only case are consistent with CBET fluid theory which is display by black line. However, in the CBET and SBS case, as shown by the green

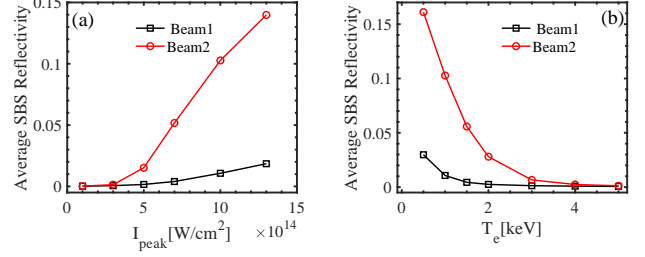


FIG. 9. Simulation results by WEBS. (a) The average SBS reflectivity for two laser beams for different laser intensities in CBET and SBS case. (b) The average SBS reflectivity for two laser beams for different plasma temperatures in CBET and SBS case.

dots in Fig 8 (a), the CBET gain does not agree with CBET fluid theory when the intensity of laser beams are larger than  $6 \times 10^{14} \text{W/cm}^2$ , this phenomenon agrees with our predication, because the CBET is in the depletion regime as shown in Fig 3 (a), the growth of SBS will reduce the energy of Beam2.

Also, we carry out the fluid simulations with different temperatures of plasma, as shown in Fig 8 (b), the orange diamonds represent the CBET only case, they agree well with CBET fluid theory. The CBET gain does not agree with fluid theory when the plasma temperature is lower than  $2 \text{keV}$ , because this parameter space belong to the depletion regime shown in Fig 3 (a), Beam2 gain much energy from CBET, then the SBS grow faster than that in front of CBET region, the interaction of CBET and SBS results in the discrepancy between the simulation results and fluid theory. As the temperature increases, CBET move from depletion region to trivial regime, the CBET and SBS can grow independently, that is why the CBET gain agree with fluid theory again at high temperature. We note that the temperature of ions are  $T_i = 0.2T_e$ , the laser intensities are  $1 \times 10^{15} \text{W/cm}^2$  in Fig 8 (b).

The average reflectivity of SBS for CBET and SBS case are shown in Fig 9, when the intensity of laser beams are lower than  $4 \times 10^{14} \text{W/cm}^2$ , the SBS reflectivity of Beam1 and Beam2 are close to each other, means the interaction is weak. The temperature dependence of SBS reflectivity also shows the huge difference of SBS reflectivity occur in the CBET depletion region. At high temperature,  $T_e > 4 \text{keV}$ , the Landau damping of IAW in SBS is large enough to suppress SBS, which leads to weaker interaction between CBET and SBS. The simulation results agree with our theoretical analysis.

### C. PIC simulations for CBET and SBS interaction with different $ZT_e/T_i$

In the fluid region of CBET and SBS, the WEBS simulation is suitable for discussing CBET and SBS interaction, it can not discuss the nonlinear kinetic effects, such as ion trapping, nonlinear Landau damping of IAWs, when the laser intensities are high enough, and  $ZT_e/T_i \leq 6$ , the kinetic effects will become important. it is necessary to use PIC simulations to prove our conclusion.

In the PIC simulations, two Gaussian type laser beam enter into the simulation box with crossed angle  $31^\circ$ , the peak intensity of laser is  $I_0 = 2.0 \times 10^{15} \text{W/cm}^2$ . The SBS seed level is  $5 \times 10^{-4} I_0$ . In Fig 10 (a), the electron temperature is 1keV, so, the parameter locate at the depletion regime of CBET which leads to strong interaction between CBET and SBS. As shown in Fig 10, the energy of Beam2 is transferred to SBS's reflected light, the SBS reflectivity of Beam2 is much higher than Beam1. At around 20ps, we observe that the SBS was saturated, then the interaction between CBET and SBS becomes weaker. The reason of saturation is the strong laser filamentation instability(not show here).

In Fig 10 (c) and (d), the electron temperature keeps same, we only change the ion temperature to  $T_e/3$ , as we know, we Landau damping of IAWs are sensitive to  $ZT_e/T_i$ , the distance between  $C_s$  and ion thermal velocities is small for low  $ZT_e/T_i$ , the Landau damping will increase significantly. The Landau damping of IAW in SBS is much larger than that in CBET process, because the wavenumber of IAW in SBS is larger. Thus, the SBS reflectivity decreases in  $ZT_e/T_i = 6$  comparing with that in  $ZT_e/T_i = 10$  case, and the interaction between CBET and SBS become weaker. In Fig 10 (e) and (f), we change the  $ZT_e/T_i$  to 3, the SBS processes is strongly damped, and the interaction between CBET and SBS can be ignored.

#### IV. CONCLUSION AND DISCUSSION

In this paper, first we construct a wave based simulation model that can be used to study the laser plasma instabilities call WEBS, this program use Du Fort-Frankel scheme to solve nonlinear Schrödinger equations. Our code has a good accuracy even with few spatial mesh. And we have benchmark our code against PIC simulations in fluid regime. Then we study the interaction of CBET and SBS in homogenous, we propose that at trivial regime, the SBS growth won't affect CBET gain, however, at the depletion regime, the CBET gain will be influence by SBS, which leads to the huge difference of SBS reflectivity for Beam1 and Beam2, and the huge SBS reflectivity will reduce the CBET gain. We use fluid simulations to prove our predications. At last, we also use PIC simulations to study the CBET SBS interaction with different  $ZT_e/T_i$ , we find that, higher  $ZT_e/T_i$  leads to strong interaction between CBET and SBS, the interaction becomes weaker with low  $ZT_e/T_i$  because of the large Landau damping of IAWs.

In ICF experiments, there are hundreds of laser beams was injected to hohlraum, In the region of beam overlap, the interaction between laser plasma instabilities should get attention, because the thresholds of instabilities will decrease under multi-beam configuration. In the future work, we will study the muti-beam SBS in the inhomogenous plasma, in this model, the interaction of CBET and SBS still exists.

#### V. ACKNOWLEDGEMENTS

We are pleased to acknowledge useful discussions with Q. Wang, Y. G. Chen, S. Tan and W. B. Yao. This work

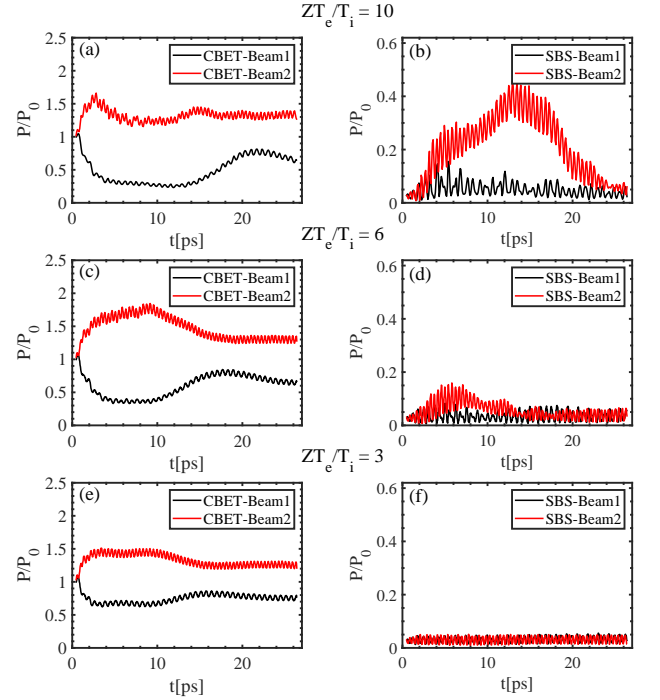


FIG. 10. The PIC simulation results. (a) the time -dependent laser beam energy in CBET and SBS case.(b)the time -dependent SBS reflectivity in CBET and SBS case.

was supported by the Scientific Research Foundation for High-level Talents of Anhui University of Science and Technology (Grant No.2022yjrc106), the Strategic Priority Research Program of Chinese Academy of Sciences (Grant No.XDA25050700), National Natural Science Foundation of China (Grant Nos.11975059),and Natural Science Foundation of Hunan Province, China (Grant No.2020JJ5029).

#### Appendix A: The Du Fort-Frankel Scheme in WEBS

In this paper, the full time steps of waves are denoted by  $n-1, n, n+1$ , and the half time steps of waves are denoted by  $n-1/2, n+1/2, n+3/2$ . space is discretized by  $\Delta x$  and  $\Delta y$  at two dimensions, for simplicity, we use  $\Delta x = \Delta y = h$ , space points are denoted by  $(i, j)$ . The Du Fort-Frankel scheme has three folds in time, which mean that the value of  $u^{n+1}$  requires  $u^n$  and  $u^{n+\frac{1}{2}}$ . For example, The Du Fort-Frankel scheme for pump laser is

$$\begin{aligned}
 a_{0,(i,j)}^{n+1} &= \frac{1-2\xi_0}{1+2\xi_0} a_{0,(i,j)}^n + \frac{\xi_0}{1+2\xi_0} \left[ a_{0,(i-1,j)}^{n+\frac{1}{2}} \right. \\
 &\quad \left. + a_{0,(i+1,j)}^{n+\frac{1}{2}} + a_{0,(i,j-1)}^{n+\frac{1}{2}} + a_{0,(i,j+1)}^{n+\frac{1}{2}} \right] \\
 &\quad + \frac{\Delta t}{1+2\xi_0} \left[ \frac{i}{2} (1-n_0) a_{0,(i,j)}^{n+\frac{1}{2}} + \frac{i}{4} \tilde{n}_{e,(i,j)}^{n+\frac{1}{2}} a_{1,(i,j)}^{n+\frac{1}{2}} \right],
 \end{aligned} \tag{A1}$$

where  $\xi_0 = \frac{i\Delta t}{2h^2}$ . Similarly, the Du Fort-Frankel scheme for seed laser is

$$\begin{aligned} a_{1,(i,j)}^{n+1} &= \frac{1-2\xi_1}{1+2\xi_1} a_{1,(i,j)}^n + \frac{\xi_1}{1+2\xi_1} \left[ a_{1,(i-1,j)}^{n+\frac{1}{2}} \right. \\ &\quad \left. + a_{1,(i+1,j)}^{n+\frac{1}{2}} + a_{1,(i,j-1)}^{n+\frac{1}{2}} + a_{1,(i,j+1)}^{n+\frac{1}{2}} \right] + \\ &\quad \frac{\Delta t}{1+2\xi_1} \left[ \frac{i}{2} \left( \frac{\omega_1^2}{\omega_0^2} - n_0 \right) a_{1,(i,j)}^{n+\frac{1}{2}} + \frac{i}{4} \tilde{n}_{e,(i,j)}^{*n+\frac{1}{2}} a_{0,(i,j)}^{n+\frac{1}{2}} \right], \end{aligned} \quad (\text{A2})$$

where  $\xi_1 = \frac{i\omega_0\Delta t}{2\omega_1 h^2}$ . The Du Fort-Frankel scheme for IAW is a little more complicated, which is

$$\begin{aligned} \tilde{n}_{e,(i,j)}^{n+1} &= \frac{1-C_1-C_2}{1+C_1+C_2} \tilde{n}_{e,(i,j)}^n + \frac{C_1+C_4}{1+C_1+C_2} \tilde{n}_{e,(i+1,j)}^{n+\frac{1}{2}} \\ &\quad + \frac{C_1-C_4}{1+C_1+C_2} \tilde{n}_{e,(i-1,j)}^{n+\frac{1}{2}} + \frac{C_2+C_5}{1+C_1+C_2} \tilde{n}_{e,(i,j+1)}^{n+\frac{1}{2}} \\ &\quad + \frac{C_2-C_5}{1+C_1+C_2} \tilde{n}_{e,(i,j-1)}^{n+\frac{1}{2}} + \frac{C_3+C_7+C_8}{1+C_1+C_2} \tilde{n}_{e,(i,j)}^{n+\frac{1}{2}} \\ &\quad + \frac{C_6}{1+C_1+C_2} \left[ \frac{4(T_{(i-1,j)} + T_{(i+1,j)} + T_{(i,j-1)} + T_{(i,j+1)})}{h^2} \right. \\ &\quad \left. + \frac{T_{(i-1,j-1)} + T_{(i+1,j+1)} + T_{(i-1,j+1)} + T_{(i+1,j-1)}}{h^2} - \frac{20T_{(i,j)}}{h^2} \right], \end{aligned} \quad (\text{A3})$$

where  $T_{(i,j)} = a_{1,(i,j)}^{*n+\frac{1}{2}} \cdot a_{0,(i,j)}^{n+\frac{1}{2}}$ , the coefficients  $C_1 \sim C_8$  are

$$\begin{aligned} C_1 &= \frac{i}{2} \frac{\omega_0\Delta t}{\omega_{20}h^2} \frac{C_s^2 - V_x^2}{c^2}, C_2 = \frac{i}{2} \frac{\omega_0\Delta t}{\omega_{20}h^2} \frac{C_s^2 - V_y^2}{c^2} \\ C_3 &= \frac{i}{2} \frac{\omega_2^2\Delta t}{\omega_0\omega_{20}}, C_4 = -\frac{\omega_2\Delta t}{2\omega_{20}h} \frac{V_x}{c} \\ C_5 &= -\frac{\omega_2\Delta t}{2\omega_{20}h} \frac{V_y}{c}, C_6 = \frac{i}{4} \frac{Zn_0m_e\omega_0\Delta t}{m_i\omega_{20}} \\ C_7 &= -v\Delta t, C_8 = -i\Delta t\delta\omega. \end{aligned} \quad (\text{A4})$$

- <sup>1</sup>R. Betti, et al., Phys. Rev. Lett. **98**, 155001 (2007).(doi: [10.1103/PhysRevLett.98.155001](https://doi.org/10.1103/PhysRevLett.98.155001))  
<sup>2</sup>Max Tabak, et al., Phys. Plasmas **1**, 1626 (1994).(doi: [10.1063/1.870664](https://doi.org/10.1063/1.870664))  
<sup>3</sup>S. E. Bodner, et al., Phys. Plasmas **5**, 1901 (1998).(doi: [10.1063/1.872861](https://doi.org/10.1063/1.872861))  
<sup>4</sup>J. Lindl, Phys. Plasmas **2**, 3933 (1995).(doi: [10.1063/1.871025](https://doi.org/10.1063/1.871025))  
<sup>5</sup>V. Tikhonchuk, et al., Matter Radiat. Extremes **4**, 045402 (2019).(doi: [10.1063/1.5090965](https://doi.org/10.1063/1.5090965))  
<sup>6</sup>J. Nuckolls, et al., Nature (London) **239**, 139 (1972).(doi: [10.1038/239139a0](https://doi.org/10.1038/239139a0))  
<sup>7</sup>J. D. Lindl, et al., Phys. Plasmas **11**, 339 (2004). (doi: [10.1063/1.1578638](https://doi.org/10.1063/1.1578638))  
<sup>8</sup>E. I. Moses, et al., Phys. Plasmas, **16**, 041006 (2009).(doi: [10.1063/1.3116505](https://doi.org/10.1063/1.3116505))  
<sup>9</sup>P. Michel, et al., Phys. Rev. Lett., **102**, 025004 (2009).(doi: [10.1103/PhysRevLett.102.025004](https://doi.org/10.1103/PhysRevLett.102.025004))  
<sup>10</sup>P. Michel, et al., Phys. Plasmas, **17**, 056305 (2010). (doi: [10.1063/1.3325733](https://doi.org/10.1063/1.3325733))  
<sup>11</sup>I. V. Igumenshchev, et al., Phys. Plasmas, **17**, 122708 (2010). (doi: [10.1063/1.3532817](https://doi.org/10.1063/1.3532817))

- <sup>12</sup>A. Oudin, et al., Phys. Rev. Lett., **127**, 265001 (2021).(doi: [10.1103/PhysRevLett.127.265001](https://doi.org/10.1103/PhysRevLett.127.265001))  
<sup>13</sup>A. G. Seaton, et al., Phys. Plasmas, **29**, 042706 (2022).(doi: [10.1063/5.0078800](https://doi.org/10.1063/5.0078800))  
<sup>14</sup>A. G. Seaton, et al., Phys. Plasmas, **29**, 042707 (2022).(doi: [10.1063/5.0078801](https://doi.org/10.1063/5.0078801))  
<sup>15</sup>A. M. Hansen, et al., Phys. Rev. Lett., **126** 075002 (2021).(doi: [10.1103/PhysRevLett.126.075002](https://doi.org/10.1103/PhysRevLett.126.075002))  
<sup>16</sup>K. L. Nguyen, et al., Phys. Plasmas, **28**, 082705 (2021). (doi: [10.1063/5.0054008](https://doi.org/10.1063/5.0054008))  
<sup>17</sup>D. J. Stark, et al., Phys. Plasmas, **28**, 022702 (2021).(doi: [10.1063/5.0022091](https://doi.org/10.1063/5.0022091))  
<sup>18</sup>D. J. Stark, et al., Phys. Plasmas, **30**, 042714 (2023).(doi: [10.1063/5.0134881](https://doi.org/10.1063/5.0134881))  
<sup>19</sup>L. Yin, et al., Phys. Plasmas, **30**, 042706 (2023).(doi: [10.1063/5.0134867](https://doi.org/10.1063/5.0134867))  
<sup>20</sup>P. Neumayer, et al., Phys. Rev. Lett. **100**, 105001 (2008).(doi: [10.1103/PhysRevLett.100.105001](https://doi.org/10.1103/PhysRevLett.100.105001))  
<sup>21</sup>J. Li, et al., Phys. Rev. E **101**, 033206 (2020).(doi: [10.1103/PhysRevE.101.033206](https://doi.org/10.1103/PhysRevE.101.033206))  
<sup>22</sup>S. Zhang, et al., Phys. Rev. E **103**, 063208 (2021).(doi: [10.1103/PhysRevE.103.063208](https://doi.org/10.1103/PhysRevE.103.063208))  
<sup>23</sup>H. A. Rose and D. F. DuBois, Phys. Rev. Lett. **72**, 2883 (1994).(doi: [10.1103/PhysRevLett.72.2883](https://doi.org/10.1103/PhysRevLett.72.2883))  
<sup>24</sup>C. Z. Xiao, et al., Phys. Rev. E **104**, 065203 (2021).(doi: [10.1103/PhysRevE.104.065203](https://doi.org/10.1103/PhysRevE.104.065203))  
<sup>25</sup>L. Hao, et al., Phys. Plasmas **23**, 042702 (2016). (doi: [10.1063/1.4945647](https://doi.org/10.1063/1.4945647))  
<sup>26</sup>O. Klimo, et al., Plasma Phys. Control. Fusion **52**, 055013 (2010). (doi: [10.1088/0741-3335/52/5/055013](https://doi.org/10.1088/0741-3335/52/5/055013))  
<sup>27</sup>O. Klimo, et al., Phys. Plasmas **18**, 082709 (2011).(doi: [10.1063/1.3625264](https://doi.org/10.1063/1.3625264))  
<sup>28</sup>Q. Wang, et al., Plasma Phys. Control. Fusion **61**, 085017 (2019).(doi: [10.1088/1361-6587/ab2736](https://doi.org/10.1088/1361-6587/ab2736))  
<sup>29</sup>Q. Wang, et al., Plasma Phys. Control. Fusion **60**, 025016 (2018).(doi: [10.1088/1361-6587/aa98bb](https://doi.org/10.1088/1361-6587/aa98bb))  
<sup>30</sup>M. N. Rosenbluth, Phys. Rev. Lett. **29**, 565 (1972). (doi: [10.1103/PhysRevLett.29.565](https://doi.org/10.1103/PhysRevLett.29.565))  
<sup>31</sup>M. N. Rosenbluth, et al., Phys. Rev. Lett. **31**, 1190 (1973).(doi: [10.1103/PhysRevLett.31.1190](https://doi.org/10.1103/PhysRevLett.31.1190))  
<sup>32</sup>J. F. Myatt, et al., Journal of Computational Physics **399**, 108916 (2019). (doi: [10.1016/j.jcp.2019.108916](https://doi.org/10.1016/j.jcp.2019.108916))  
<sup>33</sup>G. Raj, et al., Phys. Rev. Lett., **118**, 055002 (2017).(doi: [10.1103/PhysRevLett.118.055002](https://doi.org/10.1103/PhysRevLett.118.055002))  
<sup>34</sup>T. D. Arber, et al., Plasma Phys. Control. Fusion **57**, 113001 (2015). (doi: [10.1088/0741-3335/57/11/113001](https://doi.org/10.1088/0741-3335/57/11/113001))  
<sup>35</sup>Williams E A, et al., Phys. Plasmas **11** 231(2004)(doi: [10.1063/1.1630573](https://doi.org/10.1063/1.1630573))  
<sup>36</sup>Berger R L, et al., Phys. Plasmas **20**032107 (2013).(doi: [10.1063/1.4794346](https://doi.org/10.1063/1.4794346))  
<sup>37</sup>private communication with Y. G. Chen.  
<sup>38</sup>E. C. Du Fort and S. P. Franke, Mathematical Tables and Other Aids to Computation, **7** p135 (1953). (doi: [10.2307/2002754](https://doi.org/10.2307/2002754))  
<sup>39</sup>C. M. Campbell and P. Keast., Mathematics of Computation, **22**, pp. 336–346 (1968). (doi: [10.2307/2004663](https://doi.org/10.2307/2004663))  
<sup>40</sup>X. F. Yang, D. A. Ralescub, Mathematics and Computers in Simulation, **181**, pp. 98–112 (2021). (doi: [10.1016/j.matcom.2020.09.022](https://doi.org/10.1016/j.matcom.2020.09.022))  
<sup>41</sup>L. X. Wu, SIAM Journal on Numerical Analysis, **33**, pp. 1526–1533 (1996). (doi: [10.1137/S0036142994270636](https://doi.org/10.1137/S0036142994270636))  
<sup>42</sup>X. D. Hang, Mathematica Numerica Sinica, **37**: 273–285 (2015). (doi: [10.12286/jssx.2015.3.273](https://doi.org/10.12286/jssx.2015.3.273))  
<sup>43</sup>R.D. Ruth, IEEE Trans. Nuclear Science, **30**, 2669–2671 (1983). (doi: [10.1109/TNS.1983.4332919](https://doi.org/10.1109/TNS.1983.4332919))  
<sup>44</sup>D. Donnelly, E. Rogers, Am. J. Phys., **73**, 938–945 (2005).  
<sup>45</sup>C. L. Tang, J. Appl. Phys., **37**, 2945 (1966).(doi: [10.1063/1.1703144](https://doi.org/10.1063/1.1703144))  
<sup>46</sup>W. L. Kruer, *The Physics of Laser Plasma Interactions* (Westview Press, Boulder, 2003).  
<sup>47</sup>D. R. Nicholson, *Introduction to Plasma Theory* (John Wiley & Sons, New York, 1983).  
<sup>48</sup>Q. S. Feng, et al., Plasma Phys. Control. Fusion, **62**, 045013 (2020). (doi: [10.1088/1361-6587/ab7608](https://doi.org/10.1088/1361-6587/ab7608)) (doi: [10.1119/1.2034523](https://doi.org/10.1119/1.2034523))